SATELLITE OBSERVATIONS AND MODELING OF THE POLAR IONOSPHERE UNDER CONDITIONS OF THE DOMINANT AZIMUTHAL (By) IMF COMPONENT

R. Lukianova

Space Research Institute RAS (RSI RAS)

e-mail: lukianova@cosmos.ru

Received March 06, 2025

Revised May 06, 2025

Accepted May 22, 2025

Abstract. The processes occurring in the polar cap region and depending on the IMF *By* sign are considered. The results of a comparative analysis of the distributions of field-aligned currents, auroral precipitation, ionospheric plasma convection, and electron density under conditions of northward IMF and the IMF *By* component of opposite signs are presented. The field-aligned currents and precipitating particles are obtained from the AMPERE and DMSP satellite data. The convection patterns are obtained from the SuperDARN and numerical models; the electron density is calculated using the empirical IRI and a regional numerical models. It is shown that in the northern hemisphere, disturbances are concentrated near the pole and differ significantly under opposite IMF *By* signs. Under *By*+ conditions, the precipitation intensity in the center of the polar cap is much higher than under *By*– conditions. Also, only under *By*+ does the evening convection cell dominate over the morning one, providing a circumpolar flow of the ionospheric plasma in an extended range of latitudes. The model distribution of the electron density in the polar cap shows the formation of a polar peak if *By*+, and a depletion if *By*–, which corresponds to the direction of field-aligned currents and the structure of precipitation. If *By*+, a 'cyclone'-type structure is formed in the northern polar ionosphere, in which the energy and momentum of the solar wind are effectively transferred to the ionosphere during several hours of the northward IMF.

Keywords: *high-latitude ionosphere, field-aligned currents, auroral presipitation, interplanetary magnetic field*

DOI: 10.31857/S00167940250512e5

1. INTRODUCTION

The southward-directed interplanetary magnetic field (IMF) promotes the direct injection of more solar wind (SW) energy into the magnetosphere through reconnection processes at the low-latitude daytime magnetopause, where the IMF is antiparallel to the geomagnetic field. At the same

time, the polar cap expands and the auroral oval shifts to lower latitudes. When the MMP is directed northward (*Bz*+), the magnetosphere becomes "closed", the transfer of energy and momentum of the NE to the magnetosphere through reconnection is limited to a small region of high latitudes. Energy is delivered through the boundary layers of the magnetosphere via quasi-viscous interaction. This type of CB-magnetosphere interaction causes geomagnetic and auroral activity to be concentrated in the polar caps. From optical observations, it is known that during the northern MMP near the pole, daytime auroras caused by electron ejections often appear [Frey et al., 2003; Korth et al., 2004].

The concept of the role of the azimuthal, *By*, component of the IMF was formulated in [Nishida, 1971; Leontyev and Lyatsky, 1974]. During the motion from the Sun of the MMP frozen in the solar wind plasma, an electric field $\mathbf{E}_{CB} = -\mathbf{V} \times \mathrm{B}$ is generated (**V** is the solar wind velocity vector and **B** is the MMP induction; the coordinate system is fixed relative to the Earth). The vertical (north-south) component of $\mathbf{E}_{NE}$is due to the MMP *By.* Thus, at $By \neq 0$, a tension is created between the northern and southern lobes of the magnetosphere, and a potential difference is created between the ionospheres of the opposite polar caps. The *By*+ MMP (positive direction from morning to evening) generates an electric field directed in the magnetosphere from south to north. *By*– this field is directed north-south.

Longitudinal currents (LT) flowing along the highly conducting force lines of the geomagnetic field due to the interhemispheric potential drop are localized in the polar cap in the region of the daytime casp. The direction and intensity of these PTs are determined by *the* sign and magnitude of the IMF *By.* At *By*- in the northern (southern) cap, the PT flows into the ionosphere (flows out of it). At *By*+ the direction of the currents is reversed. The current system is closed by interhemispheric PTs in the area of closed force lines of the geomagnetic field. Polar structures were indeed detected in the statistical model of PTs constructed from data of the Oersted satellite [Papitashvili et al., 2002; Lukyanova et al., 2010], as well as Iridium [Anderson et al., 2008].

In the polar ionosphere, the PTs connected with *By* form a horizontal, radially directed (relative to the geomagnetic pole) electric field under the action of which the circumpolar flow of ionospheric plasma occurs. In the Northern and Southern hemispheres, the direction of plasma drift is opposite. In the northern polar cap the IMF *By*+ creates a clockwise (westward) plasma flow, and at By- the ionospheric plasma drifts counterclockwise. A linear relationship between the drift velocity and the magnitude of MMP *By* was in the measurements of the EISCAT incoherent scattering radar located in Svalbard [Lukianova and Kozlovsky, 2011]. Oppositely directed plasma flows are localized inside the polar caps in the region of (quasi-)open in the solar wind force lines of the geomagnetic field.

The specificity of the processes in the high-latitude ionosphere is a large variability depending on a number of factors. The concept of MMP *By* assumes a symmetric mirror image of the distribution of electrodynamic parameters between hemispheres with a change of sign (or direction) at positive and negative polarity *By*. However, the energetics of the processes can be different. First of all, it is determined by the intensity of auroral precipitations. Since the current carriers are electrons, in the outflowing PT from the ionosphere, the electron flux is directed from the magnetosphere downward into the ionosphere. The inflow PT is formed by less energetic ionospheric electrons or ions. This paper is devoted to the comparison of satellite observations of longitudinal currents and outflows and the results of model calculations of convection patterns and electron concentration distributions in the northern polar ionosphere under the conditions of the northern MMP By and opposite polarities of the MMP *By*.

1. PERIODS OF STABLE IMF *By*+ AND By-

The effects of the IMF *By* are most clearly manifested in the conditions of stable northern IMF. In summer 2014, two sufficiently long periods with large values of *By*+ and *By*- were observed. Fig. 1 shows the hourly values of MMP *Bz* and *By* and Kr index for the day 20.08.2014 and from 12 UT 14.07 to 12 UT 15.07.2014. In both cases, the MMP was directed to the north during the day. On August 20 (Fig. *1a*) at 06-12 UT the magnitude of *By* was about +4 nTL, and after 12 UT it increased to +13 nTL. On July 14 (Fig. *1b*) at 12 UT , the polarity of *By* changed to negative, and by the beginning of the next day, the magnitude of *By* reached -11 nTl. For the analysis, we chose 3-hour intervals with approximately the same conditions but with opposite signs of the MMP *By*: (1) 15 - 18 UT, *By* = +13 nTl, *Bz* = +9 nTl, *Kr* = 1; (2) 22 - 01 UT, *By* = -11 nTl, *Bz* = +6 nTl, *Kr* = 2. The solar wind speed was low in both cases. Such conditions are favorable for the formation of high-latitude disturbances.

Fig. 1.

Fig. 2.

2. LONGITUDINAL CURRENT AND AURORAL PRECIPITATIONS

Fig. 2 shows maps of PTs and auroral luminosity intensity in the LBH emission observed in the northern high-latitude region approximately in the middle of each of the periods of prolonged *By*+ (Fig. *2a*) and By- (Fig. *2b*). The distribution of large-scale PTs is derived from AMPERE project data from 10-min measurements of magnetic field variations by engineering magnetometers of the Iridium satellite constellation consisting of about 70 low-orbit polar spacecraft (spacecraft). The bottom panels of Fig. 2 show maps of polar auroras observed by the Defense Meteorological

Satellite Program DMSP F18 satellite over the northern hemisphere at approximately the same time points (at 17:06 and 00:42 UT, respectively) as the PTs presented in the top row of Fig. 2. The observations were made with the *Special Sensor Ultraviolet Spectrographic Imager* (SSUSI) in the *Lyman-Birge-Hopfield* (LBH) LBH band at wavelengths of 140-150 nm. DMSP satellites are in a sun-synchronous orbit; orbital period 101 min, nominal altitude 830 km.

Under *By*+ conditions, 17:20-17:30 UT, 20.08.2014 (Fig. *2a*), in the center of the polar cap, an outflowing PT with a density of more than 1.5 μA/m^2 is observed. At the noon meridian, a low-latitude PT of the opposite direction maintains the continuity of the current in the ionosphere. In the period 00:20-00:30 UT, 15.07.2014 under By- conditions in the near-pole region, an inflow PT is formed. It is closed by the outflow PT, which is located to the south at the meridian ~09 MLT. The longitudinal currents in the center of the cap lasted for several hours and transformed into a classical zone 1 structure as the MLT turned southward. DMSP F18 observed bright emissions and a large energy flux of ejected particles near the north magnetic pole just in the region of the outflowing ionospheric PT (~12 MLT). The diameter of the central spot is on the order of hundreds of kilometers. In the evening side at latitudes 70-85° MLat one can see the edge of the zone of precipitations, the maximum of which is located in the pre-midnight sector. Approximately the same pattern of eruptions was observed during the entire period *By*+ on this day.

At *By*-, 00:20-00:30 UT, 15.07.2014 (Fig. *2b*), when an inflow PT is formed in the near-pole region, there are practically no rashes in the center of the cap. The picture of auroral luminosity at 00:42 UT is typical for the level of geomagnetic activity during this period. In the area of the auroral oval, the luminosity of 250-300 Rl in the LBH emission is registered.

Fig. 3.

In Fig. 3 presents the energy characteristics - total energy flux and average energy - measured by the *Sensor Precipitating Electron and Ion Spectrometer* (SSJ) auroral particle sensor along the F18 orbital segment, images of which are shown in Fig. *2a* (*By*+) and Fig. *2b* (*By*-). The SSJ/4 and SSJ/5 versions of the instruments record both electrons and ions in the 30 eV-30 keV energy range [Redmon et al., 2017]. The differential energy fluxes obtained from each of the 10 channels are summed to obtain an integral energy flux. It is then divided by the number of observed counts to obtain the average electron and ion energy [Hardy et al., 2008]. An archive of daily SSJ digital data files of mean energy and total energy flux is available through the portal (http://www.ngdc.noaa.gov/stp/satellite/dmsp/). Differential energy flux diagrams are available graphically through NASA Goddard Space Flight Center's online data analysis system (https://cdaweb.gsfc.nasa.gov/). Appendix A presents the DMSP F18 diagrams for the considered intervals 17:30-17:15 UT 20.08.2014 (Figure A1) 00:35-00:50 UT 15.07.2014 (Figure A2). The

first diagram confirms that in the center of the cap there are fluxes of high-energy electrons and ionic precipitates are completely absent. The second diagram shows fluxes of low-energy particles shifted to auroral latitudes and very weak precipitations in the cap.

Fig. A1// appendix

Fig. A2// annex

In Fig. *3a* (*By*+) it can be seen that when the spacecraft crosses the zone of the near-pole ascending PT, the energy flux and the average energy of the ejected electrons increase significantly. The peak value for electrons at latitudes 86-87° MLat reaches 10^{12} –10^{13} eV/(cm^2-sr-c), which is two to three orders of magnitude higher than the total level in the auroral zone. This value is comparable to the flux observed during large magnetic storms [Shiokawa et al., 2013; Wing et al., 2013]. Thus, the polar ionosphere receives a sufficiently large amount of energy and flux during the extremely quiet geomagnetic state. The maximum of the energy flux observed near the center of the outflowing PT is accounted for by electrons up to 6 keV. Such electrons can penetrate the *F* region of the ionosphere [Newell et al., 1996]. At the edges, down to~ 75° MLat the softer electrons with energies of 1-2 keV are expelled. Thus, the fluxes and energies that caused the intensifications at different latitudes are different. The LBH intensity calculation for the F18 17:00-17:10 UT flyby shows that I(LBH) was ~6 kRL at 17:07 UT and ~1 kRL at 17:04 UT (http://sd-www.jhuapl.edu). Ion precipitations are observed equatorward of the polar cap boundary. They are absent in the zone of the outflowing PT.

Fig. *3b* shows the parameters of precipitations for a flyby under *By*- conditions, when in the center of the cap the PT flows into the ionosphere. In this case, the integral energy flux of electrons is an order of magnitude smaller. In the near-pole region, their average energy does not exceed 0.1 keV and increases to 1.5 keV only below 75° MLat. At auroral latitudes, an increasing flux of relatively energetic ions is also observed. Thus, the By- MMP conditions are characterized by much weaker precipitations than *By*+.

3. STRUCTURE OF THE IONOSPHERIC PLASMA CONVECTION TRAJECTORIES

In a collisionless plasma, the presence of an electric field transverse to the magnetic field is manifested in the convective drift of the plasma. The electric potential distribution in the ionosphere can be represented as a system where the convection trajectories are identical to equipotentials. To calculate the pattern of ionospheric plasma convection, a numerical model of the global distribution of the ionospheric electric potential was used [Lukianova and Christiansen, 2006]. The model contains blocks of longitudinal currents and auroral precipitations and, taking into account the electrodynamic coupling of the hemispheres, reproduces the convection patterns for the given input

parameters: solar zenith angle (seasonal and diurnal variations), *Bz*- and By-components *of* the MMP, the level of solar and geomagnetic activity. Of the empirical models, the best known is the convection model based on the comparison of the values of the electric potential measured by the DE2 satellite with the corresponding values of the MMP [Weimer, 1995]. The model is available through an online calculation portal.

Fig. 4.

Fig. 4 presents the electric potential distributions according to the numerical (Fig. *4a, b*) and empirical (Fig. *4c, d*) models for conditions as close as possible to those of the events considered on 20.08.2014 and 15.07.2014. Both models reproduce similar structures of two-vortex convection. Depending on the sign of *By,* either the morning or the evening vortex expands. The asymmetry is manifested in the fact that at *By*+ (*By*-) a larger cell of negative (positive) electric potential confirms that the outflowing (in-flowing) PT is surrounded by a circular convection flow in which the plasma rotates clockwise (counterclockwise). Nor is there any mirroring of the equipotential structure when the *By* sign changes. The expanded evening cell at *By*+ is significantly more powerful than the expanded positive cell at *By*-. In the first case, the potentials at the center of the positive and negative cells are correlated as -30/+14 kV (numerical model) and -40/+15 kV (empirical model). In the second case, the picture is much more symmetric with a ratio of -24/+20 kV and -30/+25 kV.

4. ELECTRON CONCENTRATION DISTRIBUTIONS IN THE F-LAYER

At high latitudes, the distribution of electron density (*Ne*) inhomogeneities is controlled by two main electrodynamic processes. It is determined by the electric field of magnetospheric origin, which causes plasma tubes to drift along equipotentials. The second factor is auroral rashes, which (in addition to solar UV) enhance ionization. The main source of precipitations is the plasma layer of the magnetosphere, so the particle fluxes are usually limited to the night sector of local time within the auroral oval. At a given moment of time, the combined action of the MMP, the solar zenith angle, the level of solar and geomagnetic activity creates a complex ionospheric response, which can be considered as a superposition of different effects.

Fig. 5.

The *Ne* distribution in the *F-region* of the polar ionosphere was calculated using a numerical model that takes into account the changing structure of convection trajectories depending on the MMP [Uvarov and Lukianova, 2015]. The upper row of Fig. 5 presents isoline maps of the maximum *Ne* values in the *F2* layer (*NmF2*) calculated for the conditions realized at 17 UT 20.08.2014 and 01 UT 15.07.2014. In the summer season, the main source of ionization is solar radiation. Nevertheless, some large-scale inhomogeneities stand out against this background.

A comparison of the *NmF2* distribution maps shows that at *By*+ (Fig. *5a*), a spot of enhanced ionization, on the order of $8 \cdot 10^5$ cm^{-3}, forms at ~80° MLat near 15 MLT . The peak corresponds to the electron spikes and intense auroral glow observed by DMSP and emanating from the ionospheric PT from AMPERE data. In the central cap, the model shows plasma depletion and polar hole formation. For the By- conditions (Fig. *5b*) and the poleward flowing PT into the ionosphere, the model *Ne* distribution shows only a decrease in the plasma density in the center of the cap, which is characteristic of the northern direction of the MMSP. It is difficult to say how real the fine structure predicted by the numerical model based on physical representations is. However, it can be seen that, in general, at *By*+, the polar ionosphere is characterized by greater ionization and more inhomogeneous structure than at By-.

To compare the modeling capabilities of the polar ionosphere, the bottom row of Fig. 5 presents *NmF2* maps calculated from the empirical IRI (*International Reference Ionosphere*) model [Bilitza et al., 2022]. Due to the lack of observation sites, IRI represents the high-latitude ionosphere in a very general form. The inhomogeneous structure in the polar cap is not reproduced. The model shows the variation of *NmF2* due to seasonal (July and August) and UT-dependent illumination variation. Due to the terminator shift in the Northern Hemisphere, the illuminance is maximum at 16:40 UT, which is close in time to the moment 17 UT 20.08.2014 (Fig. *5c*). On the contrary, the moment 01 UT 15.07.2014 (Fig. *5d*) is closer to the daily minimum of illuminance at 04:40 UT.

5. DISCUSSION OF THE RESULTS

The complex of satellite observation data and modeling results show that under the conditions of the northern IMF and large values of *By*+ , an effective channel is formed for the transmission of solar wind energy and momentum to the ionosphere. The intense outflowing PT formed at the center of the polar cap implies sufficiently large longitudinal electric fields and potential differences on the order of 10 kV [Knight, 1973; Johnson et al., 1998]. Under these conditions, electrons can be accelerated to ~10 keV, which is sufficient to produce auroral luminosity. The precipitating electrons form an intense auroral luminosity in the polar cap observed by DMSP on 20.08.2014 in the region of the spot of the outflowing PT. The circular shape of this glow differs from the arcs of auroral auroras that occur in the regions of outflowing PTs in the auroral oval [Kozlovsky et al., 2009; Haerendel et al., 2012; Wu et al., 2017]. The shape of the glow is also different from the large- and small-scale transpolar arcs that can appear in the polar cap at the northern MMP. Transpolar arcs are thought to occur on both closed and open geomagnetic field lines, although the mechanism for accelerating particles to energies high enough to produce glows is not entirely clear

[Hosokawa et al., 2020]. Rarer phenomena - auroras associated with fluxes of polar rain electrons with energies < 1 keV, can appear in the center of the polar cap [Reichert, 2024]. However, the intensity of such glows is much weaker than those observed on 20.08.2014.

Under the conditions of negative polarity of the IMF *By* and, correspondingly, of the PT flowing into the polar ionosphere, the energy of the auroral processes is significantly lower and the luminescence is practically not registered. The energy flux of ions (mainly protons) is weaker than that of electrons, and the contribution to the PT from the ejected ions is small. Energetic protons are not the dominant energy source in the high-latitude region.

It should be noted that there is still no consensus on the interpretation of the observations of the *Wu* MMP effects in the polar cap. Thus, Trondsen et al. [1999] concluded from the images obtained with the Viking UV camera in March-November 1986 that the increased intensity of daytime polar auroras is more often associated with $By-$, rather than $By+$. Statistical analysis of TIMED/GUVI spectrograph images of the auroras showed that their overall intensity does not change with the orientation of the IMF *By,* but there are differences between the pre- and post-midday sectors [Liou and Mitchell, 2019]. In the northern hemisphere, the energy flux in the afternoon sector is more focused and the peak value is 10% greater in *By*- conditions compared to $By+$. An opposite but weaker response to the orientation of the MMP *By is* found in the pre-midday sector.

The PT intensity depends on the Pedersen conductivity of the ionosphere. The considered events differ slightly in the dipole inclination angle and the illumination of the northern polar cap: the date 15.07.2014 is closer to the summer solstice, and 20.08.2014. - to the autumnal equinox. Studies of seasonal changes of PT conducted on a large array of satellite data showed that the current density in the most illuminated summer high-latitude ionosphere is 1.5-1.8 times higher than in the unilluminated winter ionosphere [Christiansen et al., 2002]. Based on these estimates, a temporal difference of one month should not have a large effect on the observed asymmetry in the PT distribution. The diurnal variation in conductivity also contributes to the equalization of the conditions of the two events. The terminator displacement has the greatest influence on the PTs near the morning-afternoon meridian, i.e., on the PTs of zone 1. Here, estimates of the amplitude of the UT variation in current density give approximately 10% for the solstice and up to 25% for the equinox [Lukianova and Christiansen, 2008]. The currents on the day side are less dependent on UT. But in general, for both events, the trends of seasonal and diurnal variation of illuminance are opposite, which minimizes the possible effect of ionospheric conductivity in the observed asymmetry of the PT distribution.

Longitudinal currents and associated particle ejections are responsible for the ionization and heating processes in the thermosphere/ionosphere system. It is possible to estimate the influence of the IMF *By* on the change of the plasma density (*Ne*) in the high-latitude ionosphere only approximately. Due to the absence of an observational network in the polar cap, the widely used empirical models actually exclude these latitudes from consideration. In the event-specific calculations, the numerical model predicts an increase in *NmF2* under *By*+ conditions. However, we cannot exclude that some of the small-scale inhomogeneities are artifacts. Calculations for the synthesized input parameters have shown that the polarity of the *By* MMP is crucial for the shift and extension of the ionization tongue to the morning or evening side [Lukianova et al., 2017]. Coupled SWARM satellite and incoherent scattering radar measurements showed that the plasma density locally increases at the site of the PT flowing out of the ionosphere [Lukianova, 2023]. We could not find events in which we could reliably identify the local decrease of *Ne* associated with the outflowing PT.

The convection patterns also indicate differences in the electrodynamics of the high-latitude ionosphere at opposite signs of the IMF *By*. Under *the By*+ conditions, the evening cell (with negative potential) dominates over the morning cell, providing a circumpolar clockwise flow of the ionospheric plasma. At the same time, the morning convection vortex is compressed and weakened. Note that since the electric field of convection can penetrate from the polar caps into the region of closed force lines, the azimuthal drift of plasma can propagate from the summer hemisphere to the winter hemisphere [Lukianova and Christiansen, 2006]. At the same time, the penetration efficiency also depends on the plasma dynamics in the opposite hemisphere. *Under* By- conditions, the morning and evening vortices are much more symmetric. The morning cell extends only slightly to the evening side, and the circumpolar drift is localized in the near-pole region.

Satellite observations and modeling testify in favor of the concept of the IMF *By* effect as the generation of the electric field along the north-south line, the appearance of the potential difference between the opposite polar caps and the system of interhemispheric longitudinal currents [Nishida, 1971; Leontyev and Lyatsky, 1974]. Another (and quite common) explanation of the *By* effect in the asymmetry of convection patterns is the specific configuration of reconnecting magnetic force lines and the corresponding electric field mapping into the ionosphere. It is hypothesized that during *By*+ (*By*-) magnetic reconnection occurs between the IMF and open geomagnetic field lines in the lobes of the tail of the magnetosphere behind the casp behind the casp in the post(pre)-midnight sector [Cowley and Lockwood, 1992; Zhang et al., 2021]. In the framework of this approach, one can expect a symmetric change of ionospheric parameters at the change of *By* sign, modulated to a small extent *by the* seasonal course of the Earth's dipole tilt [Reistad et al., 2021].

According to the results of [Anderson et al., 2008], the intense PTs known as the NBZ system (consisting of a pair of PTs at 85° MLat– ingress and egress at 09 and 15 MLT, respectively [Iijima et al., 1984]) may be more intense than zone 1 currents. Depending on the sign of the *Wu* MMP, either morning or evening PT is enhanced. In contrast to the "mirror symmetric" effects in the contrast events of 20.08.2014 (*By*+) and 15.07.2014 (*By*-), a global asymmetry with a greater intensity of electrodynamic and plasma processes in the polar cap under *By*+ conditions is observed in the Northern Hemisphere. At the same time, the unipolar PT and the glow spot caused by the expulsion of energetic particles are concentrated near the noon meridian.

7. CONCLUSION

Under the conditions of the northern MMP and opposite signs of the azimuthal component of the MMP (*By*+ and *By*–), the distribution of longitudinal currents, auroral precipitations, ionospheric plasma convection and electron concentration showed the following significant differences:

The luminescence intensity in the polar cap tends to increase at *By*+ and decrease at *By*-. The characteristics of the luminescence are consistent with the distribution of currents observed at different signs of *the* By-component *of* the MMP. The shift of the polar cap boundaries in the morning or evening MLT sectors also depends on the *By* sign.

At the *By*+ conditions in the center of the polar cap, an outflowing from the ionosphere longitudinal current and intense luminescence due to the increased fluxes of electrons with energies up to several keV were observed. The evening convection cell dominated over the morning one providing the circumpolar drift of the ionospheric plasma to lower latitudes. The model distribution of the electron concentration showed the formation of the near-pole peak of the plasma density, which corresponds to the direction of the longitudinal current and the structure of precipitations.

Under the By- conditions, when the inflow longitudinal current was formed in the near-pole region, the energy of high-latitudinal perturbations was much lower. The electron and ion precipitations were observed only at auroral latitudes. The convection cells were almost symmetric, and the plasma density in the cap was reduced.

The general picture testify in favor of the concept of the MMP *By* effect, in the framework of which the emergence of the electric field along the north-south line, the potential difference between the opposite polar caps, the system of interhemispheric longitudinal currents and the circumpolar motion of plasma in the ionosphere are assumed. The observed asymmetry at opposite signs of MMP *By* is determined by the direction of the longitudinal current.

The periods when the IMF is directed northward and the geomagnetic indices remain at a low level are considered quiet. However, under these conditions, if the azimuthal component of the MMP is large, the energy entering the polar latitude ionosphere can cause significant space weather changes resulting in increased satellite retardation, disruption of high-frequency radio communications and satellite navigation.

ACKNOWLEDGEMENTS

Solar wind data were obtained through NASA's Goddard Space Flight Center portal (https://omniweb.gsfc.nasa.gov/). Longitudinal current maps and digital files from the Iridium Communications satellite constellation are provided by the AMPERE Data Science Center through support from the U.S. National Science Foundation (https://ampere.jhuapl.edu/). Images of auroral emissions of the SSUSI DMSP instrument

are collected in the Johns Hopkins University Applied Physics Laboratory portal section (https://ssusi.jhuapl.edu/gallery_AUR). An archive of daily digital data files for the mean energy and total energy flux of the SSJ sensor is available through the NOAA National Centers for Environmental Information portal https:(//www.ncei.noaa.gov/data/dmsp-space-weather-sensors/access/). Graphical files of differential energy fluxes are provided by NASA's Goddard Space Flight Center's NASA Coordinated Data Analysis Web (CDAWeb) web service (https://cdaweb.gsfc.nasa.gov/). NASA's Community Coordinated Modelling Center online calculation service allowed calculations using the Weimer-1995 (https://kauai.ccmc.gsfc.nasa.gov/instantrun/weimer/) and IRI (https://kauai.ccmc.gsfc.nasa.gov/instantrun/iri/) models.

FUNDING

The work was performed within the framework of the State Assignment of the Space Research Institute of the Russian Academy of Sciences.

CONFLICT OF INTERESTS

The author declares no conflict of interest.

REFERENCES

1. *Lukyanova R. Yu., Kozlovsky A., Christiansen F.* Asymmetric structures of longitudinal currents and convection of ionospheric plasma controlled by the azimuthal component of the MMP and the season of the year // Geomagnetism and Aeronomy. V. 50. No. 5. P. 695-706. 2010.

2. *Lukyanova R.Yu.* Influence of longitudinal currents on electron concentration in the ionosphere: coupled observations of SWARM satellites and ESR radar // Space Research V. 61. No. 6. P. 466-475. 2023. https://doi.org/10.31857/S0023420623600083 .
3. *Anderson B.J., Korth H., Waters C.L., et al.* Statistical Birkeland current distributions from magnetic field observations by the Iridium constellation // Ann. Geophys. V. 26. P. 671–687. 2008. https://doi.org/10.5194/angeo-26-671-2008.
4. *Bilitza D., Pezzopane M., Truhlik V., et al.* The International Reference Ionosphere model: A review and description of an ionospheric benchmark // Rev. Geophys. V. 60. e2022RG000792. 2022. https://doi.org/10.1029/2022RG000792.
5. *Christiansen F., Papitashvili V.O., Neubert T.* Seasonal variations of high-latitude field-aligned current system inferred from Ørsted and Magsat observations // J. Geophys. Res. V. 107(A2). 2002. https://doi.org/10.1029/2001JA900104.
6. *Cowley S.W.H., Lockwood M*. Excitation and decay of solar wind-driven flows in the magnetosphere-ionosphere system // Ann. Geophys. V. 10. N 1–2. P. 103–115. 1992.
7. *Frey H.U., Immel T.J. Lu G., et al*. Properties of localized, high latitude, dayside aurora // J. Geophys. Res., V. 108. A4. 8008. 2003. https://doi.org/10.1029/2002JA009332.
8. *Haerendel G., Frey H.U., Chaston C.C., et al*. Birth and life of auroral arcs embedded in the evening auroral oval convection: A critical comparison of observations with theory // J. Geophys. Res., V. 117. A12220. 2012. https://doi.org/10.1029/2012JA018128.
9. *Hardy D.A., Holeman E.G., Burke W.J., et al*. Probability distributions of electron precipitation at high magnetic latitudes // J. Geophys. Res. V. 113. A06305. 2008. https://doi.org/10.1029/2007JA012746.
10. *Hosokawa K., Kullen A., Milan S., et al*. Aurora in the Polar Cap: A Review // Space Sci. Rev. V. 216. 15. 2020. https://doi.org/10.1007/s11214-020-0637-3.
11. *Iijima T., Potemra T.A., Zanetti L.J., Bythrow P.F.* Large scale Birkeland currents in the dayside polar region during strongly northward IMF: A new Birkeland current system // J. Geophys. Res. V. 89. P. 7441–7452. 1984. https://doi.org/10.1029/JA089iA09p07441.
12. *Johnson M.L., Murphree J.S., Marklund G.T., Karlsson T.* Progress on relating optical auroral forms and electric field patterns // J. Geophys. Res., V. 103. P. 4271–4284. 1998. https://doi.org/10.1029/97JA00854.
13. *Knight S.* Parallel electric fields // Planet. Space Sci. V. 21. P. 741–750. 1973. https://doi.org/10.1016/0032-0633(73)90093-7.
14. *Korth H., Anderson B.J., Frey H.U., et. al*. Conditions governing localized high-latitude dayside aurora // Geophys. Res. Lett. V. 31. L04806. 2004. https://doi.org/10.1029/2003GL018911.

15. *Kozlovsky A., Turunen T., Massetti S.* Field-aligned currents of postnoon auroral arcs // J. Geophys. Res. V. 114. A03301. 2009. https://doi.org/10.1029/2008JA013666.
16. *Leontyev S.V., Lyatsky W.B.* Electric field and currents connected with Y-component of interplanetary magnetic field // Planet. Space Sci. V. 22. P. 811–819. 1974. https://doi.org/10.1016/0032-0633(74)90151-2.
17. *Liou K., Mitchell E.* Effects of the interplanetary magnetic field y component on the dayside aurora // Geosci. Lett. V. 6. 11. 2019. https://doi.org/10.1186/s40562-019-0141-3.
18. *Lukianova R., Christiansen F.* Modeling of the global distribution of ionospheric electric field based on realistic maps of field-aligned currents // J. Geophys. Res. V. 111. A03213. 2006. https://doi.org/10.1029/2005JA011465.
19. *Lukianova R., Christiansen F.* Modeling of the UT effect in global distribution of ionospheric electric fields // J. Atmos. Solar-Terr. Phys. V. 70. P. 637–645. 2008. https://doi.org/10.1016/j.jastp.2007.08.047.
20. *Lukianova R., Kozlovsky A.* IMF B_y effects in the plasma flow at the polar cap boundary // Ann. Geophys. V. 29. P. 1305–1315. 2011. https://doi.org/10.5194/angeo-29-1305-2011.
21. *Lukianova R., Uvarov V.M., Coisson P*. High-latitude F region large-scale ionospheric irregularities under different solar wind and zenith angle conditions // Adv. Space Res. V. 59. № 2. P. 557–570. 2017. https://doi.org/10.1016/j.asr.2016.10.010.
22. *Newell P.T., Feldstein Y.I., Galperin Y.I., Meng C.-I.* Morphology of nightside precipitation // J. Geophys. Res. V. 101. A5. P. 10737–10748. 1996. https://doi.org/10.1029/95JA03516.
– *Nishida A.* Interplanetary origin of electric fields in the magnetosphere // Cosmic Electrodyn. V. 2. P. 350–374. 1971.
23. Papitashvili V.O., Christiansen F., Neubert T. A new model of field-aligned currents derived from high-precision satellite magnetic field data // Geophys. Res. Lett. V. 29. № 14. 1683. 2002. https://doi.org/10.1029/2001GL014207.
24. *Redmon R.J., Denig W.F., Kilcommons L.M., Knipp D.J.* New DMSP database of precipitating auroral electrons and ions // J. Geophys. Res. Space Physics. V. 122. P. 9056–9067. 2017. https://doi.org/10.1002/2016JA023339.
25. *Reichert S.* Polar rain // Nat. Phys. V. 20. 1057. 2024. https://doi.org/10.1038/s41567-024-02595-w.
26. *Reistad J.P., Laundal K.M., Østgaard N., et al.* Quantifying the lobe reconnection rate during dominant IMF B_y periods and different dipole tilt orientations // J. Geophys. Res. Space. V. 126. e2021JA029742. 2021. https://doi.org/10.1029/2021JA029742.

27. *Shiokawa K., Yumoto K., Meng C.-I., Reeves G.* Broadband electrons observed by the DMSP satellites during storm-time substorms // Geophys. Res. Lett. V. 23. № 18. P. 2529–2532. 2010. https://doi.org/10.1029/96GL01955
28. *Trondsen T.S., Lyatsky W., Cogger L.L., Murphree J.S.* Interplanetary magnetic field By control of dayside auroras // J. Atmos. Solar-Terr. Phys. V. 61. P. 829-840. 1999. https://doi.org/10.1016/S1364-6826(99)00029-2.
29. *Uvarov V.M., Lukianova R.Yu.* Numerical modeling of the polar F region ionosphere taking into account the solar wind conditions // Adv. Space Res. V. 56. P. 2563–2574. 2015. https://doi.org/10.1016/j.asr.2015.10.004.
30. *Weimer D.R.* Models of high-latitude electric potentials derived with a least error fit of spherical harmonic coefficients // J. Geophys. Res. V. 100. A10. P. 19595–19607. 1995. https://doi.org/10.1029/95JA01755.
31. *Wing S., Gkioulidou M., Johnson J.R., et al*. Auroral particle precipitation characterized by the substorm cycle // J. Geophys. Res. –Space Phys. V. 118. P. 1022–1039. 2013. https://doi.org/10.1002/jgra.50160.
32. *Wu J., Knudsen D.J., Gillies D.M., et al.* Swarm observation of field-aligned currents associated with multiple auroral arc systems // J. Geophys. Res. – Space Phys. V. 122. P. 10145–10156. 2017. https://doi.org/10.1002/2017JA024439.
33. *Zhang Q.H., Zhang Y.L., Wang C., et al.* A space hurricane over the Earth's polar ionosphere // Nat. Commun. V. 12. 1207. 2021. https://doi.org/10.1038/s41467-021-21459-y.

FIGURE CAPTIONS

Fig. 1. *Bz-* and *By-components of* MMP and Kr-index (*a*) 20.08.2014 and (*b*) 14-15.07.2014. The time interval with a particular *By* sign is highlighted by shading.

Fig. 2. Ionospheric projection of PT AMPERE (top row) and intensity of DMSP optical emissions (bottom row) in the Northern Hemisphere in MLT - MLat coordinates: (*a*) 17:06 UT 20.08.2014 at By+ and (*b*) 00:42 UT, 15.07.2014 at By– . Adapted from (https://ampere.jhuapl.edu/) and (https://ssusi.jhuapl.edu/gallery_AUR).

Fig. 3. Integral energy flux and average energy of electrons and ions along the orbit of DMSP F18 (*a*) 17:01-17:12 UT, 20.08.2014 and (*b*) 00:36-00:47 UT, 15.07.2014.

Fig. 4. Electric potential distribution from the numerical model (top row) and the Weimer model (bottom row) for conditions (*a, c*) *By* = +12 nTl, *Bz* = +8 nTl, *Kp*= 1, DOY= 232 and (*b, d*) *By* = -12 nTl, *Bz* = +8 nTl, *Kp*= 1, DOY= 1 92. MLT-MLat coordinate system; difference between equipotentials of 2 kV and 5 kV; potential values at the center of the convection cells are indicated at the bottom of each diagram.

Fig. 5. Distribution of *NmF2* (10^5el/cm^3) by numerical model (top row) and by IRI model (bottom row) for conditions *Bz* = +8 nTl and (*a, c*) *By* = +12 nTl, 17 UT, 20.08.2014 and (*b, d*) *By* = -12 nTl, 01 UT, 15.07.2014.

Appendix A

FIGURE CAPTIONS APPENDICES

Fig. A1. Differential energy fluxes of electrons and ions along the DMSP F18 flyby trajectory in the interval 17:30-17:15 UT 20.08.2014; the lower plots show the change in magnetic latitude and MLT (source: https://cdaweb.gsfc.nasa.gov/).

Fig. A2. The same for the interval 00:35-00:50 UT 15.07.2014.

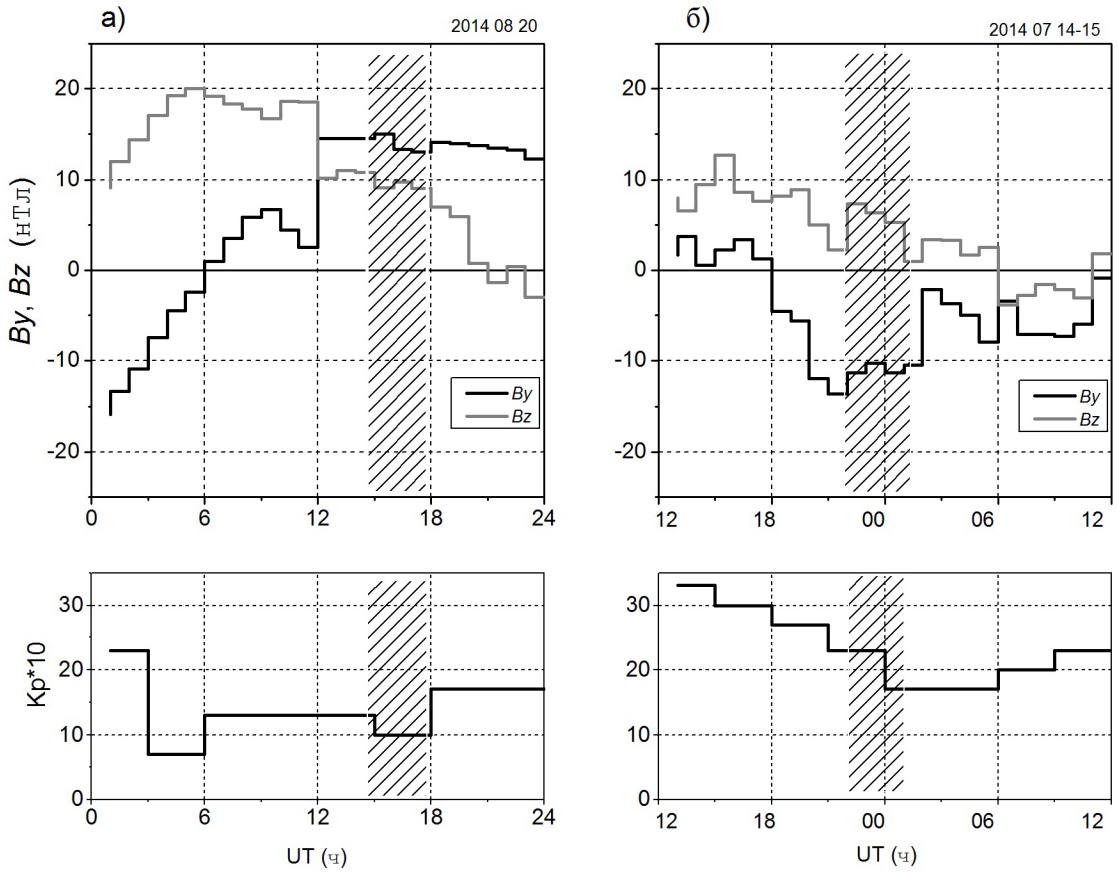

Fig. 1.

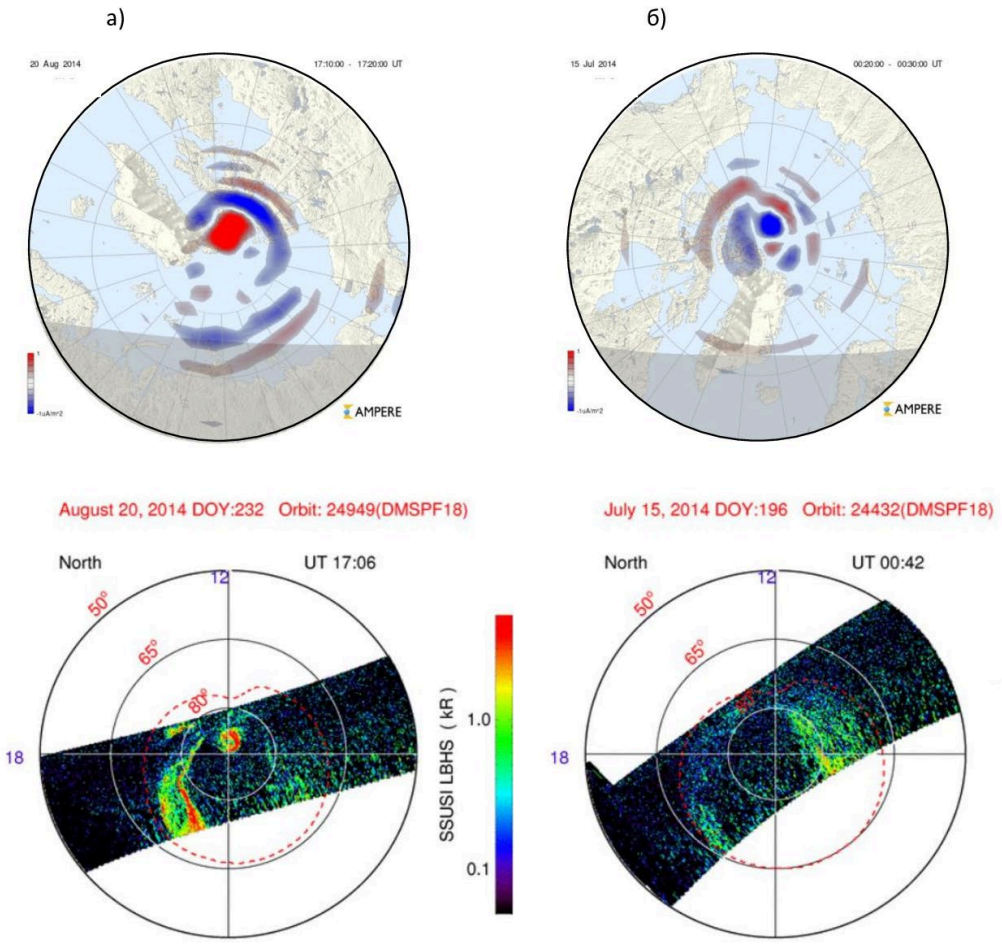
а)
б)
20 Aug 2014
17:10:00 - 17:20:00 UT
15 Jul 2014
00:20:00 - 00:30:00 UT
AMPERE
AMPERE
August 20, 2014 DOY:232 Orbit: 24949(DMSPF18)
July 15, 2014 DOY:196 Orbit: 24432(DMSPF18)
North
UT 17:06
North
UT 00:42
12
18
50°
65°
80°
SSUSI LBHS (kR)
1.0
0.1

Fig. 2.

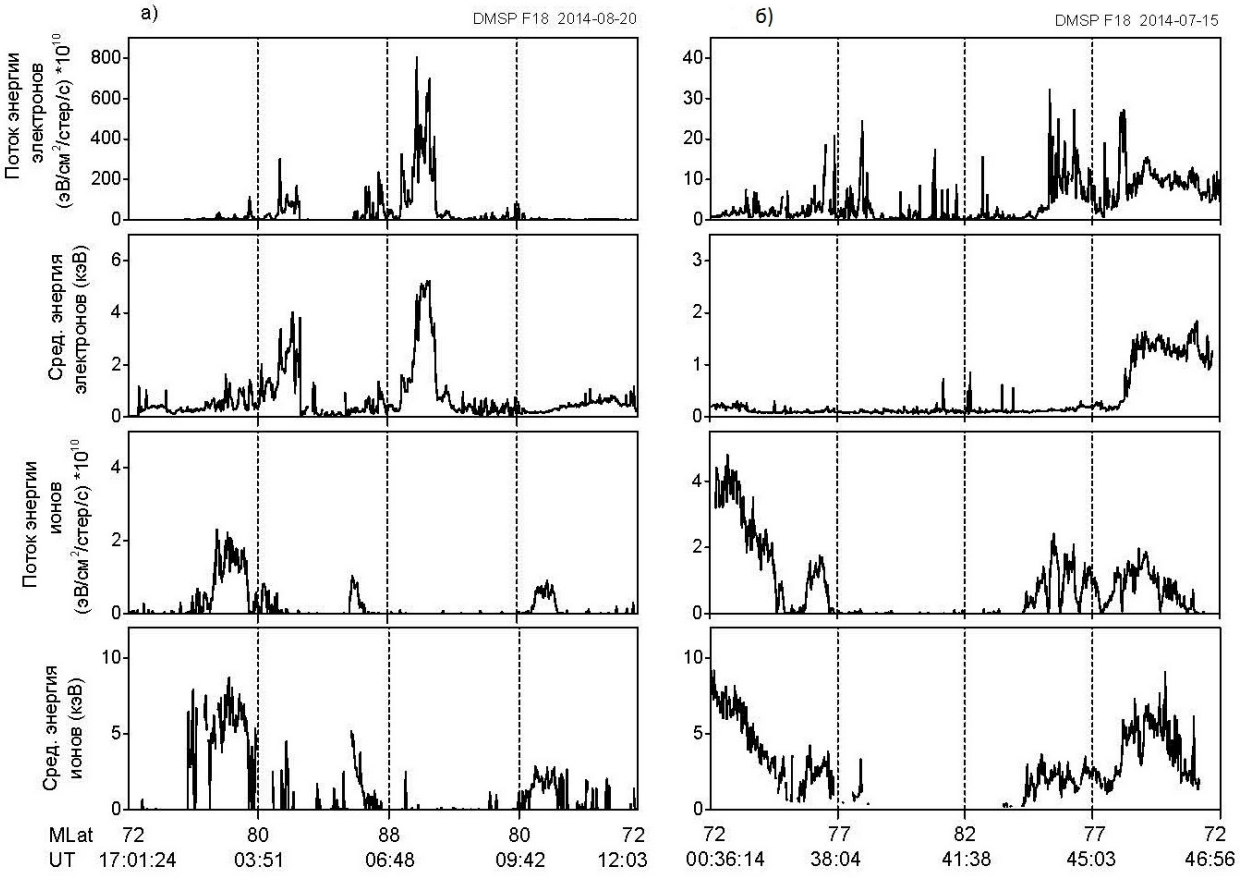
а)
DMSP F18 2014-08-20
б)
DMSP F18 2014-07-15
Поток энергии электронов (эВ/см²/стер/с) *10¹⁰
Сред. энергия электронов (кэВ)
Поток энергии ионов (эВ/см²/стер/с) *10¹⁰
Сред. энергия ионов (кэВ)
MLat 72 80 88 80 72
UT 17:01:24 03:51 06:48 09:42 12:03
72 77 82 77 72
00:36:14 38:04 41:38 45:03 46:56

Fig. 3.

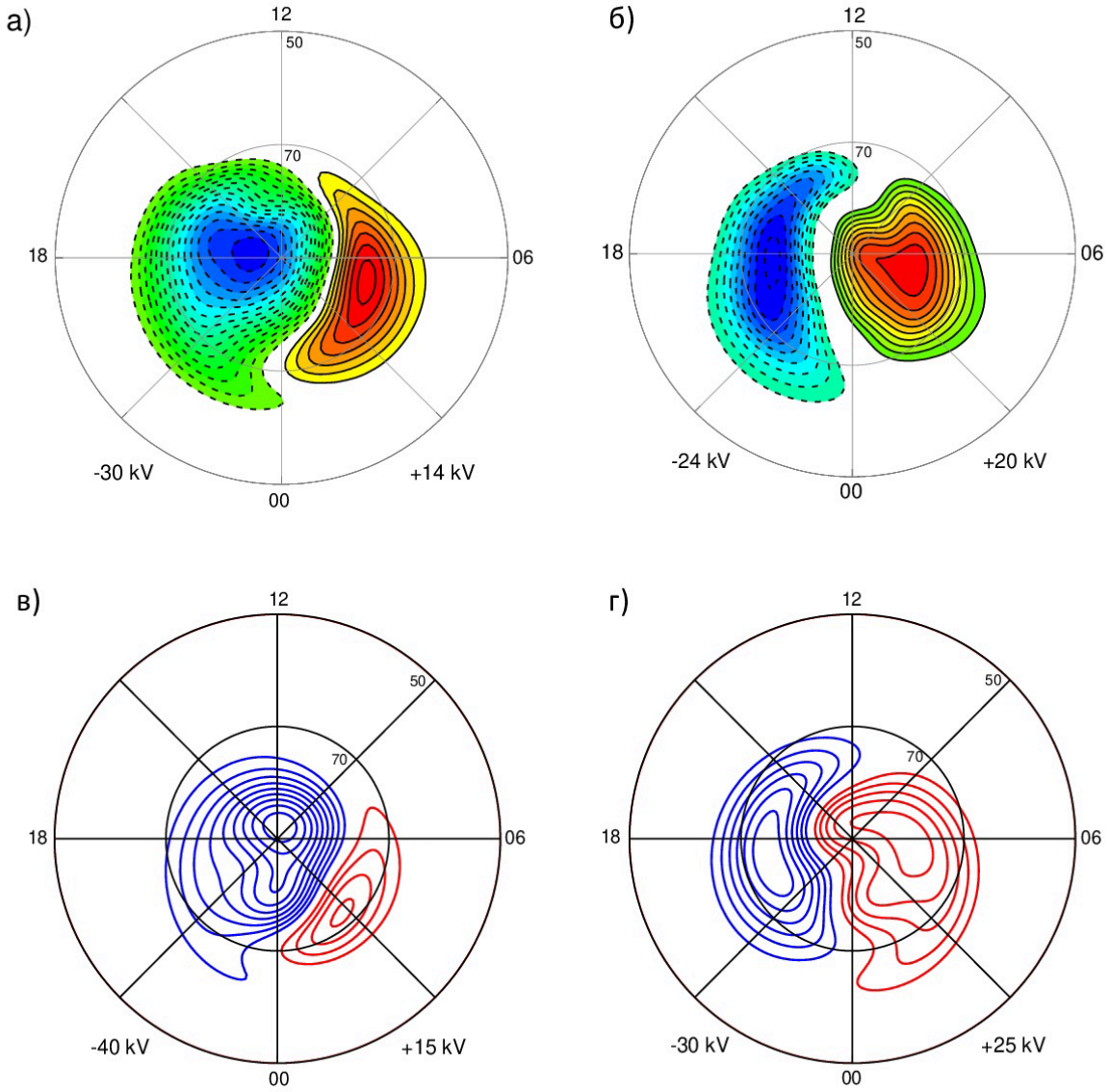
а)
12
50
70
18
06
-30 kV
+14 kV
00
б)
12
50
70
18
06
-24 kV
+20 kV
00
в)
12
50
70
18
06
-40 kV
+15 kV
00
г)
12
50
70
18
06
-30 kV
+25 kV
00

Fig. 4.

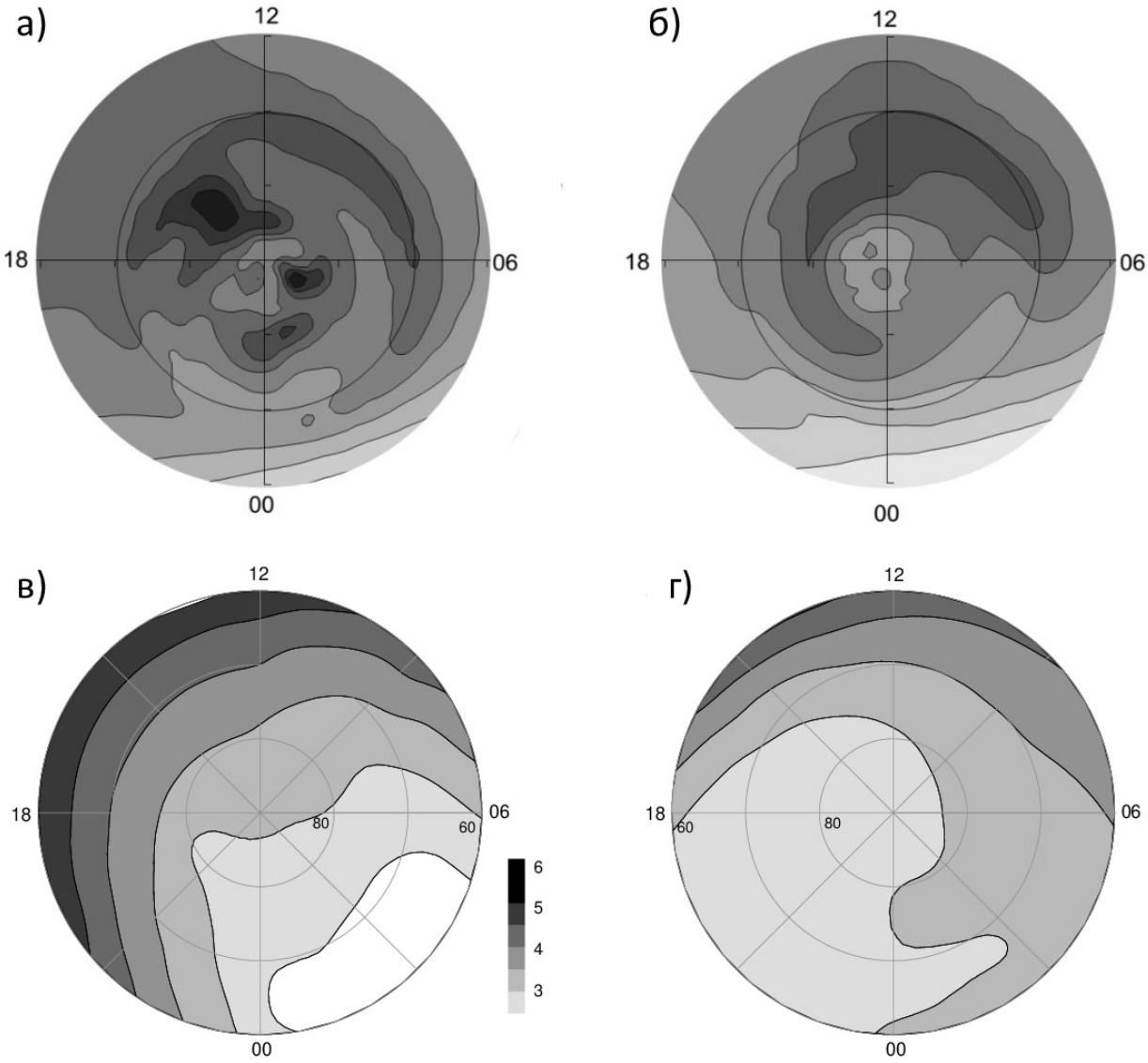

Fig. 5.

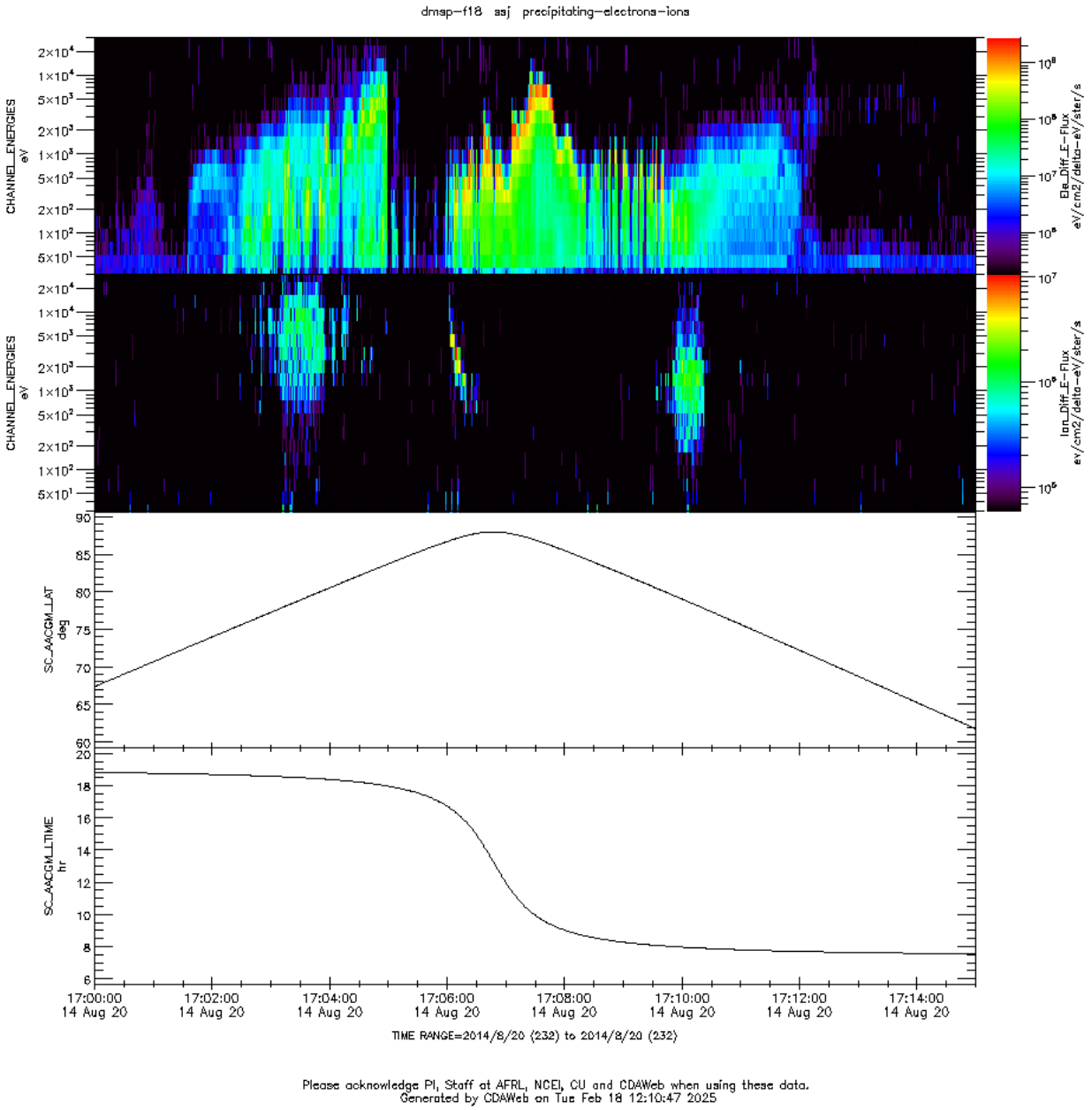

Fig. A1. (appendix)

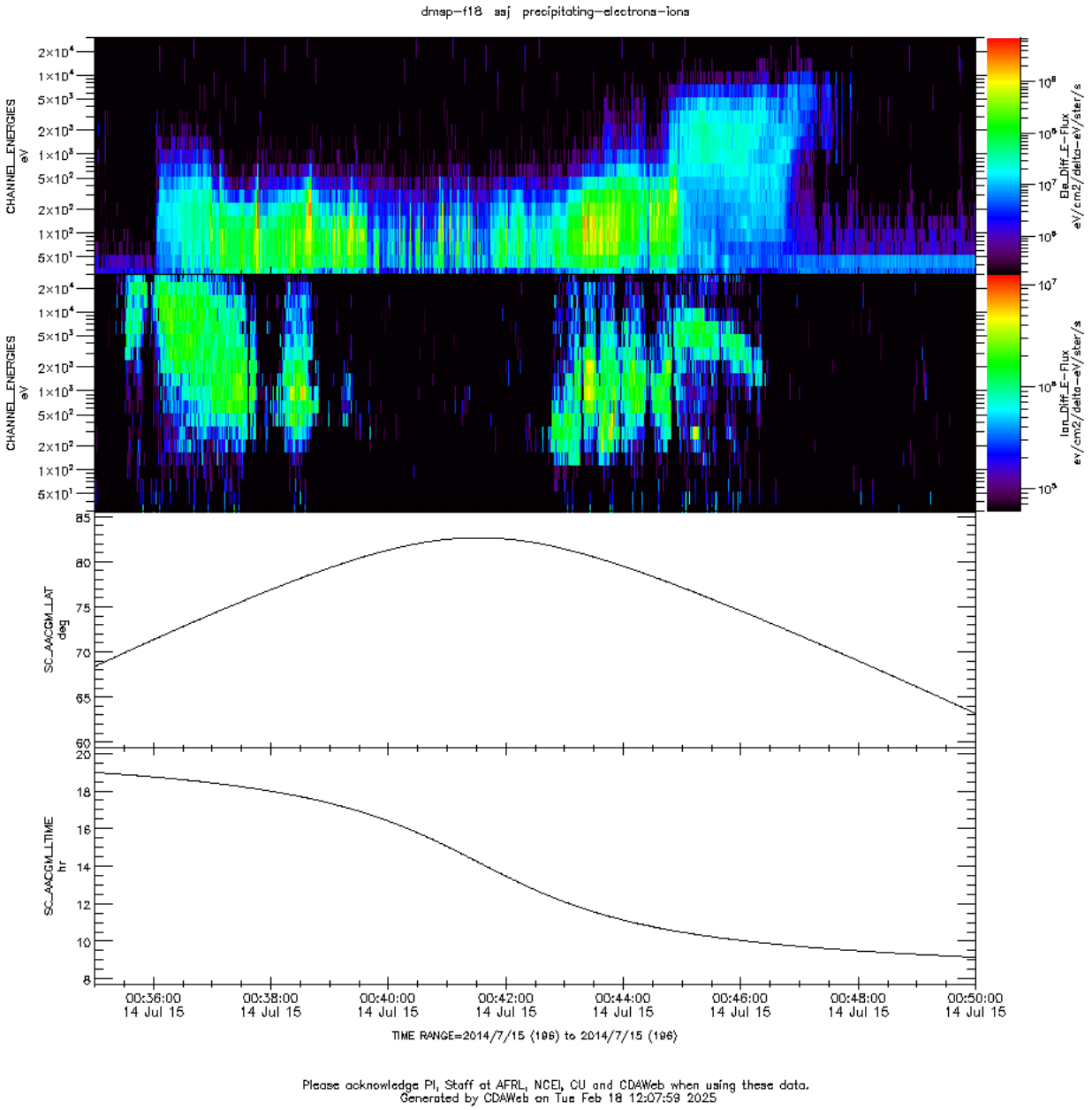

Fig. A2. (appendix)